Journal of Southeast University (English Edition) Vol. 32, No. 1, pp. 67 - 72 Mar. 2016 ISSN 1003—7985

Strength calculation methodology for internally ring-stiffened DT-joints

Wang Fan[1,2] Lan Xiaoyi[2] Pan Xiaorong[2,3] Ning Chen[2]
Xu Xiaofeng[2] Liu Dingding[2] Luo Zhifeng[2]

([1] State Key Laboratory of Subtropical Building Science, South China University of Technology, Guangzhou 510640, China)
([2] Architectural Design and Research Institute, South China University of Technology, Guangzhou 510640, China)
([3] Shanghai Municipal Engineering Design Institute (Group) Co., LTD, Shanghai 200092, China)

Abstract: In order to obtain the strength design equations for internally ring-stiffened circular hollow section tubular DT (double tee)-joints subjected to brace axial compression or tension, theoretical and numerical studies on 800 stiffened joints were conducted. Based on the failure mechanism of the stiffened joints, four theoretical models and corresponding equations for predicting the strength of the stiffeners are proposed. Combined with existing unstiffened DT-joint design equations, a design equation for the stiffened joints is proposed. The finite element analysis shows that the failure of the stiffened joints under brace axial loads can be characterized by plastic hinges forming in the stiffener and chord wall yielding in the vicinity of the brace-chord intersection. The reliability of the proposed stiffener strength equations is demonstrated by a reliability analysis. Good agreement is achieved between the stiffened joint strength calculated from the proposed joint strength equation and that obtained from finite element analysis.

Key words: double-tee joint; ring-stiffener; failure mechanism; ultimate strength

DOI: 10.3969/j.issn.1003 - 7985.2016.01.012

Tubular joints are major load-carrying structural components in onshore and offshore tubular structures. There is relatively extensive research on the strength of unstiffened tubular joints[1-3]. Design equations for unstiffened tubular joints are available in major steel structure design guides.

Tubular joints are often strengthened by internal ring stiffeners. In spite of the significance of this type of strengthened joints, there is relatively little research on the determination of the strength of internally ring-stiffened tubular joints. Thandavamoorthy et al.[4] reported on the test results of T- and Y-joints reinforced with triple stiffeners and compared the strengths with their associated unstiffened joints. It is found that the strength of the stiffened joints was almost twice that of corresponding unstiffened joints. Lee et al.[5-6] reported a finite element study on the strength of saddle-stiffened T-joints and DT-joints subjected to brace axial compression. Mei et al.[7] tested three internally ring-stiffened DT-joints. It is found that the strength of the stiffened joints was up to 1.7 times that of corresponding unstiffened joints. Wang et al.[8] reported a finite element study on the strength of crown-stiffened T- and Y-joints subjected to brace axial compression or tension and proposed equations for predicting the strength of the stiffened T- and Y-joints. Due to the scarcity of research, design equations for internally ring-stiffened joints are still not available in major design guides.

In this paper, finite element and theoretical studies on the strength of stiffeners in crown- and saddle-stiffened DT-joints (in-plane brace angle $\theta = 90°$) subjected to brace axial compression or tension are carried out. Based on the collapse mechanism identified, four theoretical models for stiffener strength predictions are proposed. A equation for the stiffened DT-joint strength prediction is then proposed based on the summation of the stiffener strength and the unstiffened joint strength.

1 Finite Element Modeling

Fig.1 shows the stiffened DT-joint configuration and the joint geometric parameter definition. The general finite element program ABAQUS is used to carry out the finite element analysis. A four-node quadrilateral shell element S4R is used to model the unstiffened and stiffened

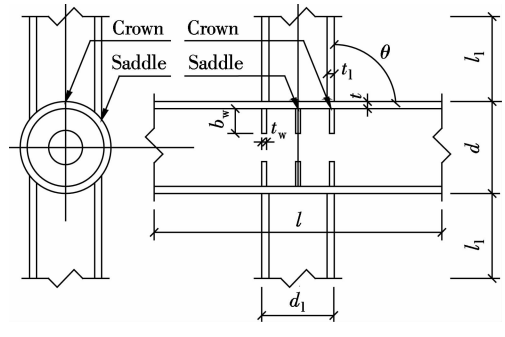

Fig. 1 Internally ring-stiffened DT-joint configuration

Received 2015-09-14.

Biography: Wang Fan (1971—), male, doctor, associate professor, wangfan@scut.edu.cn.

Foundation item: The Open Project of State Key Laboratory of Subtropical Building Science, South China University of Technology (No. 2014KB29, 2015ZB30).

Citation: Wang Fan, Lan Xiaoyi, Pan Xiaorong, et al. Strength calculation methodology for internally ring-stiffened DT-joints[J]. Journal of Southeast University (English Edition), 2016, 32(1): 67 - 72. DOI: 10.3969/j.issn.1003 - 7985.2016.01.012.

DT-joints. The mesh size of the joints is carefully determined by a convergence study. It is found that the mesh size of approximately 20 mm for all joints can produce accurate joint strength predictions with a reasonable computational cost. A five-point integration through the shell thickness is adopted.

The adopted material curve of steel Q345B which is commonly used in the Chinese construction industry is an elastic-perfectly plastic curve with yield stress f_y = 345 MPa and yield strain ε_y = 0.001 67. The value of the Poisson's ratio is 0.3. The material and geometric nonlinearities are taken into account. The weld modeling is not included due to its insignificant effect on joint strengths[6]. Fig. 2 shows the boundary conditions and loading modes. One end of the chord is given a fixed boundary condition and the other end is constrained to displace along the chord axis. The brace axial translation and three rotations are unconstrained with the other two translations being restricted. The brace axial compression and tension loadings are applied by displacement at the brace ends. The loads are applied in increments by using the "Static" method in the ABAQUS library.

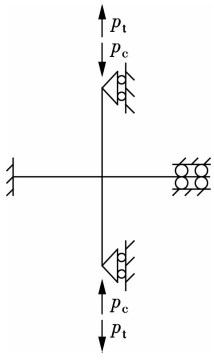

Fig. 2 Boundary conditions and loading modes

To validate the finite element (FE) modeling of the stiffened DT-joints adopted in this paper, the published unstiffened and ring-stiffened DT-joint strength data in Refs. [6 − 7] (N_{Ref}) is compared with the joint strength obtained from the finite element analysis (N_{FE}). The results of this validation study are shown in Tab. 1. It can be seen that the strengths of all six joints have been predicted to well within 10% of the literature results. This level of accuracy confirms the validity of the finite element modeling adopted. It should be noted that the strength of the stiffened DT-joints is determined by the peak load or deformation limit ($0.03d$) in load-displacement curves. If the deformation at the peak load is smaller than $0.03d$, then the peak load is considered to be the joint strength. If the deformation at the peak load is larger than $0.03d$, then the load at the deformation of $0.03d$ is considered to be the joint strength.

Tab. 1 Results of the validation study

Joint	N_{FE}/kN	N_{Ref}/kN	N_{FE}/N_{Ref}
DT-W(0.4, 0.2)[a][6]	9 288	8 616	1.08
DT-W(0.6, 0.2)[a][6]	10 460	9 589	1.09
DT-W(0.8, 0.2)[a][6]	11 250	10 543	1.07
Specimen 1[7]	3 580	3 900	0.92
Specimen 2[7]	5 778	5 300	1.09
Specimen 3[7]	5 904	6 200	0.95

2 Strength Prediction

The stiffened joint strength can be considered as the sum of the strengths of the unstiffened joint and of the stiffener[6]. Thus, the strength of the stiffener in each joint analyzed (ΔN_X) is calculated by subtracting from the stiffened joint strength (N_X) the corresponding unstiffened joint strength (N_X^{pj}). The ranges of parameters which are common in joints occurring in engineering practice are shown in Tab. 2. It should be noted that for saddle-stiffened DT-joints, only one stiffener is positioned at the saddle. For crown-stiffened DT-joints, each crown position is stiffened with one stiffener.

Tab. 2 Ranges of DT-joint parameters analyzed in Cases 1 to 4 mm

Joint parameter	Parameter range			
	Case 1	Case 2	Case 3	Case 4
Stiffener depth b_w	80, 120, 160, 200, 240	80, 120, 160, 200, 240	80, 120, 160, 200, 240	80, 120, 160, 200, 240
Stiffener thickness t_w	16, 18, 20, 22, 24	16, 18, 20, 22, 24	16, 18, 20, 22, 24	16, 18, 20, 22, 24
Brace outer diameter d_1	300, 350, 400, 450, 500, 550, 600, 650, 700	300, 350, 400, 450, 500, 550, 600, 650, 700	300, 350, 400, 450, 500, 550, 600	300, 350, 400, 450, 500, 550, 600

Note: All joints with chord outer diameter d = 800 mm, chord wall thickness t = 20 mm, chord length l = 4 800 mm, brace wall thickness t_1 = 16 mm, brace length l_1 = 2 400 mm, in-plane brace angle θ = 90° (see Fig. 1 for joint geometric parameter definition).

2.1 Failure mechanism

In this paper, four cases as shown in Tab. 3 are studied. Figs. 3(a) to (d) show typical yielding patterns within stiffeners in the stiffened DT-joints in Cases 1 to 4, respectively. The distinct highly strained zones (in red and green color) which become plastic indicate the existence of plastic hinges in the stiffeners. These plastic hinges, therefore, suggest that bending action is the main load-carrying mechanism of the stiffeners. An area (in red color) in the vicinity of the brace-chord intersection which extends along the length of the chord wall yields in Cases 1 to 4 (see Fig. 3(e)). The above observations indicate that the stiffened DT-joints fail when the chord wall near

the brace-chord intersection yields and plastic hinges form in those highly strained areas within the stiffener. It is assumed that the stiffener and the chord wall interact in providing strength enhancement. Thus, the cross section of the plastic hinge is assumed to be that of a T-section (see Fig. 4).

Tab. 3 Summary of analyzed cases

Case studies	Brace loading	Stiffening position
Case 1	Compression	Crown
Case 2	Compression	Saddle
Case 3	Tension	Crown
Case 4	Tension	Saddle

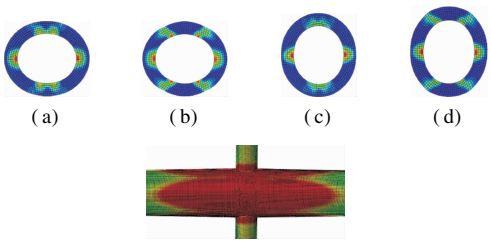

Fig. 3 Plastic zones in the stiffener and yielding area on the chord wall in Cases 1 to 4. (a) Stiffener in Case 1; (b) Stiffener in Case 2; (c) Stiffener in Case 3; (d) Stiffener in Case 4; (e) Yielding area on chord wall in Cases 1 to 4

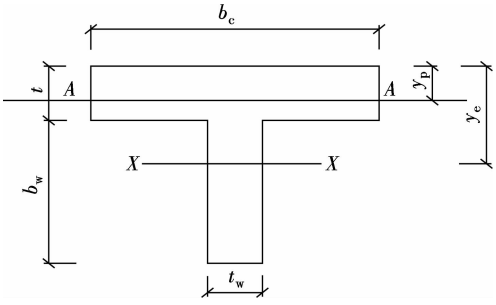

Fig. 4 T-section of the plastic hinges

2.2 Stiffener strength prediction for Case 1

2.2.1 Theoretical model

Fig. 3(a) shows that the stiffened DT-joint fails when four plastic hinges form in the stiffener. Thus, the collapse of the stiffened joints in Case 1 is assumed to be by a four-hinge failure mechanism which has both vertical and horizontal planes of symmetry. Fig. 5(a) shows the assumed location of the four plastic hinges in the theoretical model. Only the top half, above the horizontal plane of symmetry, is shown in Fig. 5(b). The straight links between the hinges as shown in Fig. 5(b) are used for the purpose of calculation convenience. The virtual work equation in Fig. 5(b) is given by

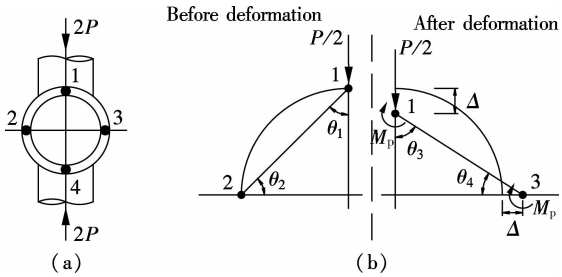

Fig. 5 A four-hinge failure mechanism. (a) Assumed location of plastic hinges; (b) Theoretical model

$$0.5P\Delta = M_p((\theta_3 - \theta_1) + (\theta_2 - \theta_4)) \tag{1}$$

where M_p is the full plastic moment resistance of the T-section (see Fig. 4); P is the strength of a single stiffener. Herein, the stiffened joint deformation limit (Δ) is assumed to be $0.03d$. The values of θ_i, $i = 1$ to 4, are given by

$$\left.\begin{aligned} &\theta_1 = \theta_2 = 45° \\ &\theta_4 = 90° - \theta_3 \\ &\theta_3 = \sin^{-1}\left(\frac{d + 2\Delta}{2l_1}\right) \\ &l_1 = d\sin\theta_1 = \frac{\sqrt{2}}{2}d \end{aligned}\right\} \tag{2}$$

The two stiffeners resist a total load of $2P$. The total stiffener strength, ΔN_X, is given by

$$\Delta N_X = 2P = \frac{8M_p(\theta_3 - \theta_1)}{\Delta} \tag{3}$$

2.2.2 Deduction for M_p

In Fig. 4, the depth of the centroidal axis X-X is given by

$$y_e = \frac{0.5(b_c t^2 + t_w b_w^2) + t t_w b_w}{A} \tag{4}$$

where the area of the T-section, A, is given by

$$A = b_c t + b_w t_w \tag{5}$$

The depth of the neutral axis is given by

$$y_p = \begin{cases} \dfrac{A}{2b_c} & 0 < y_p \leqslant t \\ \dfrac{A + 2t(t_w - b_c)}{2t_w} & t < y_p \leqslant t + b_w \end{cases} \tag{6}$$

The plastic section modulus is given by

$$W_p = \begin{cases} \left(y_e - \dfrac{A}{4b_c}\right)A & 0 < y_p \leqslant t \\ (t_w - b_c)t^2 + Ay_e - t_w y_p^2 & t < y_p \leqslant t + b_w \end{cases} \tag{7}$$

The plastic moment of resistance is given by

$$M_p = W_p f_y \tag{8}$$

2.2.3 Determination of the effective flange width

If the effective flange width, b_e, is determined, the total stiffener strength, ΔN_X, can be obtained using Eqs. (2) to (8). Using the Excel VBA program, the value of

b_c is calculated by the following iterative process. Assuming an initial effective flange width, the value of b_c is iterated until the stiffener strength calculated from Eqs. (2) to (8) is equal to the corresponding stiffener strength obtained from finite element analysis. For the ease of calculation purpose, an equation for predicting the value of b_c is proposed by investigating the effects of non-dimensional geometric parameters β ($= d_1/d$), η ($= b_w/d$) and τ ($= t_w/t$) on non-dimensional parameter b_c/d. Near quadratic relationships between b_c/d and β, η as well as τ are found, respectively. The relationship between b_c/d and γ ($= d/2t, 10 \leqslant \gamma \leqslant 30$) is linear[6]. Based on the above observations, multiple regression analyses are carried out, using the values of b_c of 225 ring-stiffened DT-joints. The equation for predicting the value of b_c is given by

$$\frac{b_c}{d} = 3.318 \times (\tau^2 - 2.622\tau + 1.157) \times (\eta^2 - 0.402\eta + 0.021)(\beta^2 - 0.975\beta + 0.284) \times (2\gamma + 63.735) \quad (9)$$

The validity ranges of Eq. (9) are as follows: $0.375 \leqslant \beta \leqslant 0.875$, $0.8 \leqslant \tau \leqslant 1.2$, $0.1 \leqslant \eta \leqslant 0.3$, $10 \leqslant \gamma \leqslant 30$, $\theta = 90°$.

2.2.4 Stiffener strength prediction

Given the geometric parameters of the ring-stiffened DT-joints, the value of b_c can be obtained using Eq. (9). This allows the determination of the plastic moment of resistance, M_p, using Eqs. (4) to (8). By substituting the values of θ_i and M_p into Eq. (3), the total stiffener strength can be readily calculated.

2.3 Stiffener strength predictions for Cases 2 to 4

Figs. 3(b) to (d) show that in Cases 2 to 4, the stiffened DT-joint fails when six, four and six plastic hinges form in the stiffener, respectively. Thus, the collapse of the stiffened joints in Cases 2 to 4 is assumed to be by a six-, four- and six-hinge failure mechanism, respectively. The postulated failure mechanisms in Cases 2 to 4 are shown in Figs. 6 to 8, respectively. Only the top half of the theoretical models are shown in Figs. 6 to 8 due to the symmetry. Tab. 4 shows a brief summary of the results of the theoretical and numerical studies on stiffener strengths in Cases 2 to 4. The validity ranges for Case 2 are $0.375 \leqslant \beta \leqslant 0.875$, $0.8 \leqslant \tau \leqslant 1.2$, $0.1 \leqslant \eta \leqslant 0.3$, $10 \leqslant \gamma \leqslant 30$, $\theta = 90°$. The validity ranges for Cases 3 and 4 are $0.375 \leqslant \beta \leqslant 0.75$, $0.8 \leqslant \tau \leqslant 1.2$, $0.1 \leqslant \eta \leqslant 0.3$, $10 \leqslant \gamma \leqslant 30$, $\theta = 90°$.

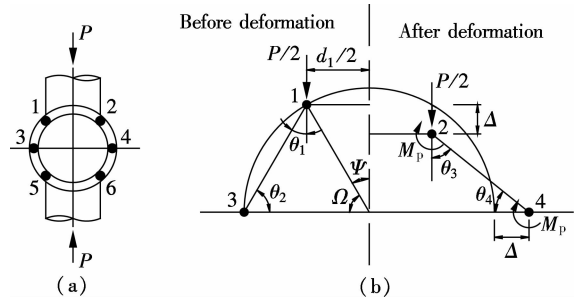

Fig. 6 A six-hinge failure mechanism in Case 2. (a) Assumed location of plastic hinges; (b) Theoretical model

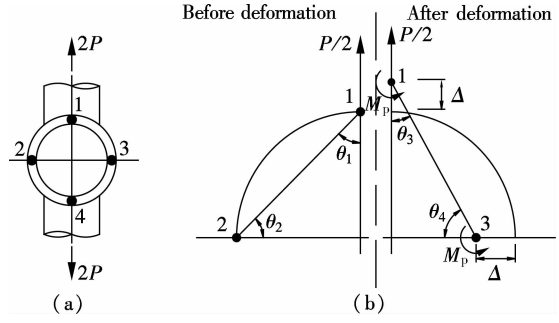

Fig. 7 A four-hinge failure mechanism in Case 3. (a) Assumed location of plastic hinges; (b) Theoretical model

Tab. 4 Results of the theoretical and numerical studies on stiffener strengths in Cases 2 to 4

Case	θ_i	b_c	ΔN_X
Case 2	$\theta_2 = 90° - \theta_1$, $\theta_4 = 90° - \theta_3$ $\psi = \sin^{-1}\left(\frac{d_1}{d}\right)$, $\theta_1 = 45° - \frac{\psi}{2}$ $l_1 = d\cos\theta_2 = d\sin\theta_1$ $\theta_3 = \sin^{-1}\left(\frac{d - d_1 + 2\Delta}{2l_1}\right)$	$\frac{b_c}{d} = 0.046(\tau + 0.198) \times (\eta^2 - 0.316\eta + 0.003) \times (\beta^2 + 24.233\beta + 18.686) \times (2\gamma - 59.201)$	$\Delta N_X = P = \frac{4M_p(\theta_3 - \theta_1)}{\Delta}$
Case 3	$\theta_1 = \theta_2 = 45°$, $\theta_4 = 90° - \theta_3$ $l_1 = d\sin\theta_1 = \frac{\sqrt{2}}{2}d$ $\theta_3 = \sin^{-1}\left(\frac{d - 2\Delta}{2l_1}\right)$	$\frac{b_c}{d} = -1.470(\tau^2 - 2.725\tau + 1.115) \times (\eta^2 - 0.419\eta + 0.022) \times (\beta^2 - 0.425\beta + 0.072) \times (2\gamma - 286.324)$	$\Delta N_X = 2P = \frac{8M_p(\theta_1 - \theta_3)}{\Delta}$
Case 4	$\theta_2 = 90° - \theta_1$, $\theta_4 = 90° - \theta_3$ $\psi = \sin^{-1}\left(\frac{d_1}{d}\right)$, $\theta_1 = 45° - \frac{\psi}{2}$ $l_1 = d\cos\theta_2 = d\sin\theta_1$ $\theta_3 = \sin^{-1}\left(\frac{d - d_1 - 2\Delta}{2l_1}\right)$	$\frac{b_c}{d} = -0.508(\tau + 7.420) \times (\eta^2 - 0.383\eta + 0.013) \times (\beta^2 - 1.514\beta + 0.330) \times (2\gamma - 133.134)$	$\Delta N_X = P = \frac{4M_p(\theta_1 - \theta_3)}{\Delta}$

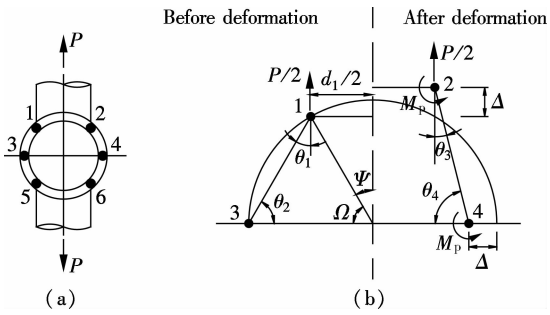

Fig. 8 A six-hinge failure mechanism in Case 4. (a) Assumed location of plastic hinges; (b) Theoretical model

The procedure of the stiffener strength calculation in Cases 2 to 4 is similar to that described in Section 2.2.4. Given the geometric parameters of the ring-stiffened DT-joints, the value of b_c can be determined using the equation of b_c as shown in Tab. 4. Thus, the plastic moment of resistance, M_p, can be determined using Eqs. (4) to (8). By substituting the values of θ_i and M_p into the equation of ΔN_X, the total stiffener strength can be obtained.

2.4 Reliability analysis

A reliability analysis was carried out to assess the reliability of the proposed stiffener strength equations in Cases 1 to 4. The reliability of the equations is measured by a reliability index, β_0. In this study, a target reliability index of 2.5 is used, according to Refs. [9 − 10]. If the value of β_0 is higher than 2.5, the equations are considered to be reliable. A resistance factor φ of 0.65 is used to calculate the value of β_0 of the proposed equations. The load combination of $1.2L_D + 1.6L_L$ specified in the ASCE Standard[11] is used in the reliability analysis. The ratio of dead load L_D to live load L_L is adopted as 0.2. The reliability index in the ASCE Standard[11] is given by

$$\beta_0 = \frac{\ln((M_m F_m P_m)/(0.657\varphi))}{\sqrt{V_M^2 + V_F^2 + C_P V_P^2 + 0.21^2}} \tag{10}$$

where the parameters are taken as $M_m = 1.10$, $F_m = 1.00$, $V_M = 0.10$ and $V_F = 0.05$, which are the mean values and coefficients of variations for material and fabrication factors, respectively. The parameters P_m and V_P are the mean value and coefficient of variation of the tested-to-predicted load ratio, respectively. A correction factor C_p in the NAS Specification[12] is adopted in the reliability analysis to consider the influence of a small number of tests. The result of statistical analysis for Cases 1 to 4 is shown in Tab. 5. Herein, the strength ratio r_{si} is defined as $N_{fi}/N_{ei}(i = 1, 2, \ldots, n)$. n is the number of the stiffened joints calculated in each case; N_{fi} and N_{ei} are the numerical and theoretical stiffener strengths, respectively.

Tab. 5 shows that the reliability indices of the proposed stiffener strength equations for Cases 1 to 4 are all higher than the target value of 2.5. Thus, the equations are able to produce reliable limit state designs.

Tab. 5 Results of statistical analysis for Cases 1 to 4

Case studies	n	Mean P_m	COV V_P	β_0
Case 1	225	1.04	0.11	3.74
Case 2	225	1.02	0.06	3.93
Case 3	175	1.02	0.10	3.72
Case 4	175	1.00	0.09	3.69

2.5 Ring-stiffened DT-joint strength

The total stiffener strength, ΔN_X, can be obtained from the proposed stiffener strength equations in Sections 2.2 to 2.3. The strength of the unstiffened DT-joints subjected to brace axial loads, N_X^{pj}, can be obtained from finite element analysis or calculated from design equations in many design codes (e.g. CECS 280: 2010[13]). Combined with existing unstiffened DT-joint design equations, a design equation for the stiffened DT-joint is proposed as

$$N_X = K_p(N_X^{pj} + \Delta N_X) \tag{11}$$

where K_p is a parameter considering the effect of chord stress. The stiffened joint strength obtained from finite element analysis ($N_{X,FEM}$) is compared with that calculated from Eq. (11) ($N_{X,Eq}$) as shown in Fig. 9. It can be seen that the value of $N_{X,Eq}$ has predicted to be well within 10% of $N_{X,FEM}$ in Cases 1 to 4. Therefore, it confirms the accuracy of Eq. (11).

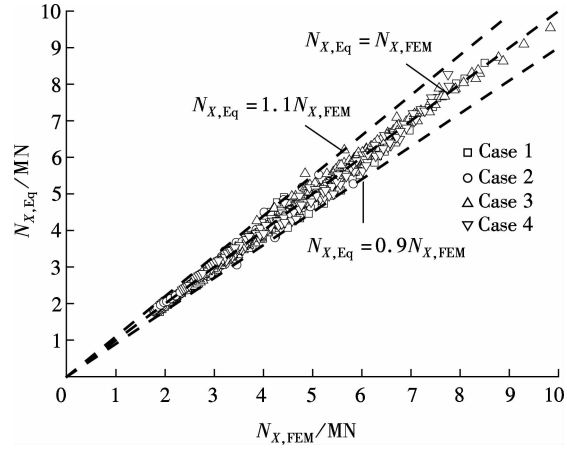

Fig. 9 Comparison between $N_{X,FEM}$ and $N_{X,Eq}$

3 Conclusion

The failure mechanism of the stiffened joints under brace axial loads can be characterized by plastic hinges forming in the stiffener and chord wall yielding in the vicinity of the brace-chord intersection.

The proposed stiffener strength equations can produce reasonable reliable limit state designs when calibrated with a resistance factor of 0.65 for the stiffened joints.

In conjunction with existing unstiffened DT-joint design equations, a design equation for the stiffened DT-joint is proposed. Good agreement is achieved between

the stiffened joint strength calculated from the proposed joint strength equation and that obtained from finite element analysis.

References

[1] Kim J W, Kim S S, Lee M J, et al. Vierendeel joints in the circular hollow sections of high strength steel subjected to brace moment and chord compressive loadings [J]. *International Journal of Steel Structures*, 2012, **12**(4): 579 – 587.

[2] Shen W, Choo Y S, Wardenier J, et al. Static strength of axially loaded elliptical hollow section X joints with braces welded to wide sides of chord. Ⅰ: Numerical investigations based on experimental tests [J]. *Journal of Structural Engineering*, 2014, **140**(1): 04013035.

[3] Shen W, Choo Y S, Wardenier J, et al. Static strength of axially loaded elliptical hollow section X joints with braces welded to wide sides of chord. Ⅱ: Parametric study and strength equations [J]. *Journal of Structural Engineering*, 2014, **140**(1): 04013036.

[4] Thandavamoorthym T S, Rao M A G, Santhakumar A R. Behavior of internally ring-stiffened joints of offshore platforms [J]. *Journal of Structural Engineering*, 1999, **125**(11): 1348 – 1352.

[5] Lee M M K, Llewelyn-Parry A. Offshore tubular T-joints reinforced with internal plain annular ring stiffeners [J]. *Journal of Structural Engineering*, 2004, **130**(6): 942 – 951.

[6] Lee M M K, Llewelyn-Parry A. Strength prediction for ring-stiffened DT-joints in offshore jacket structures [J]. *Engineering Structures*, 2005, **27**(3): 421 – 430. DOI: 10.1016/j.engstruct.2004.11.004.

[7] Mei Q, Gong J H, Pang D D, et al. Effect of internal ring-stiffened spacing on behavior for X-joints [J]. *Steel Construction*, 2011, **26**(5): 11 – 16. DOI: 10.3969/j.issn.1007-9963.2011.05.003. (in Chinese)

[8] Wang F, Chen Z J, Liu D D, et al. Calculation method for bearing capacities of internal ring-stiffened tubular T- and Y-joints [J]. *Journal of Southeast University* (*Natural Science Edition*), 2014, **44**(4): 811 – 816. DOI: 10.3969/j.issn.1001-0505.2014.04.023. (in Chinese)

[9] Feng R, Young B. Design of cold-formed stainless steel tubular T-and X-joints [J]. *Journal of Constructional Steel Research*, 2011, **67**: 421 – 436.

[10] Feng R, Young B. Theoretical analysis of cold-formed stainless steel tubular joints [J]. *Engineering Structures*, 2015, **83**: 99 – 115. DOI: 10.1016/j.engstruct.2014.10.030.

[11] American Society of Civil Engineers. Minimum design loads for buildings and other structures [S]. New York: ASCE, 2006.

[12] American Iron and Steel Institute. North American specification for the design of cold formed steel structural members [S]. Washington, DC, USA: American Iron and Steel Institute, 2007.

[13] Central Research Institute of Building and Construction Group Co., Ltd. CECS 280: 2010 Technical specification for structures with steel hollow section [S]. Beijing: China Planning Press, 2010. (in Chinese)

内置环肋正交 X 形节点承载力计算方法

王 帆[1,2] 蓝小艺[2] 潘晓荣[2,3] 宁 晨[2] 许晓峰[2] 刘丁丁[2] 罗志峰[2]

([1] 华南理工大学亚热带建筑科学国家重点实验室, 广州 510640)

([2] 华南理工大学建筑设计研究院, 广州 510640)

([3] 上海市政工程设计研究总院(集团)有限公司, 上海 200092)

摘要: 为了得到受支管轴向压力或拉力的内置环肋圆钢管相贯正交 X 形节点的承载力设计公式,对 800 个带肋节点进行了理论和有限元分析. 基于带肋节点的破坏机理,提出 4 种计算加劲肋承载力的理论模型及相应的计算公式. 结合已有的无肋正交 X 形节点的设计公式,提出带肋节点的设计公式. 有限元分析表明,受支管轴力的带肋节点破坏时,加劲肋中形成塑性铰且主支管相贯区域的主管壁屈服. 可靠度分析证明了所提出的加劲肋承载力计算公式的可靠性. 由该公式计算所得的带肋节点承载力与由有限元分析所得的带肋节点承载力吻合较好.

关键词: 正交 X 形节点;环形加劲肋;破坏机理;极限承载力

中图分类号: TU391